Exciton-model approach to fast-particle emission in heavy-ion collisions

Akira Iwamoto
Japan Atomic Energy Research Institute, Tokai, Naka-gun, Ibaraki, Japan
(Received 28 April 1986)

Emission of fast particles in low-energy heavy-ion reactions is calculated using the exciton model. The initial state of the excitons is fixed by pure momentum-space considerations. By defining the projectile source and the target source as independent emitters of the fast particles, we calculate the angle-energy double-differential cross section. Angular dependence is obtained by fixing the total linear momenta of the projectile source and target source separately in addition to fixing their excitation energies. A linear-momentum-dependent level density is used for this purpose. This model is applied to several heavy-ion reactions whose energy is 10–20 MeV per particle. Our calculations reproduce the data for the high-energy part of the energy spectra well. Our model is one way of understanding the mechanism of the moving-source model.

I. INTRODUCTION

In heavy-ion reactions with energies of several tens of MeV per particle, energetic nucleons and light composite particles are emitted more frequently than is calculated by the evaporation model. Such fast particles are identified by direct measurement or by detection of the fusion residue velocity spectra. Phenomenologically, the energy-angle double-differential cross sections can be reproduced well by the moving-source parametrization.[1,2] Theoretically, proposals such as the Fermi-jet model,[3–5] the exciton model,[6–10] the time-dependent Hartree-Fock (TDHF) model,[11,12] the Boltzmann-Uehling-Uhlenbeck (BUU) [or the Vlasov-Uehling-Uhlenbeck (VUU)] model,[13,14] and many others have been examined. By contrast with the light-ion reactions, it is ambiguous to fix configurations and trajectories of the heavy-ion projectile and the target. The models proposed up to now absorb these ambiguities in the values of parameters. We propose a new model for calculating the double-differential cross section which obviates the need for precise trajectories and configurations.

One of our purposes is to understand the physics behind the phenomenological moving-source parametrization.[1,2] The moving-source model is based on an intuitive idea and has achieved good success in explaining the data. Nevertheless, the basis of this model is not clear and it is highly desirable to understand it on more fundamental grounds. As discussed in the following sections, our model will play a role in achieving this purpose.

Our model is composed of two items: the Fermi-sphere consideration and the exciton model. The idea of the Fermi sphere is to pay attention only to the momentum-space consideration of the nucleons in the target and the projectile and neglecting all information on the configuration space. Because of this simplification, we do not need the precise trajectories of the heavy ions and their configurations. With this idea, we fix the initial condition of the exciton model which is used to calculate the double-differential cross section. This model has a relation to the Fermi-jet model[3–5] and we intend to calculate the secondary scattering of the Fermi-jet particles by the exciton model. By this procedure we hope to calculate phenomenologically the effect of the collision terms as is calculated by the BUU (or VUU) model.[13,14] The total linear momentum of the excitons brought in by the Fermi-jet particles plays a crucial role in determining the angular distribution. By fixing the values of the parameters for the exciton model as those obtained in the light-ion calculations, we can calculate the absolute values of the cross sections. Agreement with data is fairly good, as will be shown in Sec. III. A preliminary report on this subject was published in Ref. 15.

In the next section we give the motivation and formalism of our model. In Sec. III we will give the results of the numerical calculations and related discussions for the emission of protons. In Sec. IV we give a brief summary.

II. MODEL

We calculate the emission of fast nucleons in heavy-ion reactions for incident energies of several tens of MeV per nucleon. In this energy range, the main reaction channels are the fusionlike, deep-inelastic, and quasielastic processes. We formulate the model corresponding to the first channel. We pay attention to the fast particle emission, which is not taken into account by the evaporation process. Thus the process we tackle is the incomplete fusion reaction.

The Fermi-jet idea[3–5] gives a simple model with which to understand fast-particle emission. This model, however, has some problems when it is applied to the data analysis. In this model one must fix the trajectories of both heavy ions (projectile and target), which is difficult to achieve. Another point is that it is also difficult to incorporate the effect of the secondary scattering of the Fermi-jet particles. To resolve these problems we adopt the exciton model, and in order to define the initial condition of the model we use Fermi-sphere considerations. In it, we use only the momentum space.

A. Initial condition of excitons

We start with the experimental data of Refs. 16 and 17. The authors of Refs. 16 and 17 analyzed the ratio of the incomplete fusion cross section to the total fusion cross section for many reaction channels and for many incident energies. One of the conclusions of their analysis is that the velocity of the light collision partner, measured in the center-of-mass frame, is a good measure of controlling the occurrence of the incomplete fusion. The relative velocity of the projectile and the target (or equivalently the energy per nucleon) is not a good measure for describing such processes when the data for different mass asymmetry of the initial channels are compared. In Ref. 17 the data were analyzed on the basis of simple Fermi-sphere–model considerations and it was found that the center-of-mass frame (or the rest frame of the compound nucleus) is suitable as a reference frame. We adopt thus the compound nucleus as a basis of the exciton-model calculations.

The way of fixing the initial condition for the exciton-model calculation is the following. We show in Fig. 1 an example of our Fermi-sphere model for the reaction $^{16}O+^{27}Al$ for the incident energy of 315 MeV leading to the compound nucleus ^{43}Sc. In this figure we show the Fermi spheres in the momentum space of the compound nucleus ^{43}Sc (centered at C_c), the projectile ^{16}O (centered at C_p), and the target ^{27}Al (centered at C_t). The latter two are calculated at the Coulomb barrier position, thus their centers are displaced from C_c corresponding to the incoming velocities at the barrier. For simplicity, we assume the same Fermi momentum for all nuclei. Because we take the compound nucleus as a reference frame, the sphere centered at C_c is our basis. The number of states in the momentum volume $d\mathbf{p}$ at $\mathbf{p}$ for projectile ($i=p$) and target ($i=t$) is given by the Fermi-gas model as

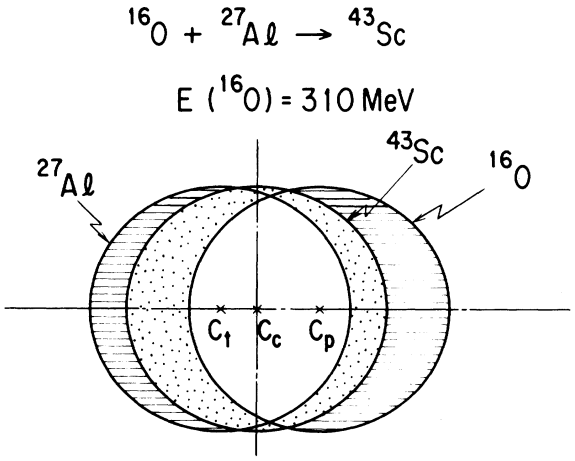

FIG. 1. Illustration of the Fermi spheres in the momentum space for the reaction 310-MeV ^{16}O on ^{27}Al. Fermi sphere of ^{16}O (centered at C_p) of ^{27}Al (centered at C_t), together with that of the compound nucleus ^{43}Sc (centered at C_c) are shown. Same Fermi energy of 33.5 MeV is assumed for all nuclei. The meaning of the shaded and dotted area is given in the text.

$$\bar{n}_i d\mathbf{p}=\frac{4V_i d\mathbf{p}}{(2\pi\hbar)^3} \quad (i=p \text{ or } t)\ , \tag{1}$$

where V_i is the volume and

$$\bar{n}_i=\frac{V_i}{2\pi^3\hbar^3}=\frac{2r_0^3A_i}{3\pi^2\hbar^3} \quad (i=p \text{ or } t) \tag{2}$$

is the density of states in momentum space expressed by the radius parameter r_0 and the mass number A_i. This density for ^{43}Sc is a sum of those for ^{16}O and ^{27}Al because the density is proportional to A. The central blank area in Fig. 1 corresponds to the situation where the densities of ^{16}O and ^{27}Al overlap. Two shaded areas in the figure are particle states, one coming from ^{16}O and the other from ^{27}Al. Two dotted areas, on the other hand, are thought to be hole states because the density of momentum space is less than the normal density for the compound nucleus. The central blank area is a 0-particle, 0-hole state in this terminology. We identify such configurations in the momentum space as initial configurations of the exciton model calculations; i.e., we use the compound basis in order to specify the state of two nuclei at the barrier top position. This does not mean, however, that the normal compound nucleus is formed at that instance. We do not use any information of the configuration space in the following exciton-model calculations. What we assume is that the composite system with a nearly spherical Fermi surface is formed. Even the dinuclear shape at the barrier will be allowed unless its Fermi sphere is much distorted.

Next, we assume that fast particles are emitted from either one of two independent sources. One is the projectile source, which is defined as the sum of particles in the right shaded area and holes in the left dotted area in Fig. 1. The other is the target source, which is defined as the sum of the left shaded and right dotted areas. The former source is so named because it is composed of projectile particles and a lack (or holes) of target particles. The linear momenta of the particles and holes in the projectile source are directed to the right direction and stand for the current from left to right. The linear momenta of the target source are directed to the left and stand for the current from right to left. These two currents mix as time proceeds and finally they stop and form the states of the compound nucleus. We assume, insofar as the nonequilibrium fast particle is concerned, that these two sources emit fast particles independently at the early stage of the reaction process.

We now calculate the particle-hole numbers, excitation energies, and total linear momenta of two sources corresponding to the situation of Fig. 1. These values are used as initial conditions of the following exciton-model calculation. The number of particles and number of holes in a source are the same because the volume of the momentum space is the same as seen clearly in Fig. 1. We denote by $N_p^{(0)}$ the exciton number (particle + hole) of the projectile source and by $N_t^{(0)}$ that of the target source. These are obtained from the integration of

$$N_i^{(0)}=\bar{n}_i\int_i d\mathbf{p} \quad (i=p \text{ or } t)\ , \tag{3}$$

where the integration is performed for the sum of shaded

and dotted areas for the projectile source or the target source. These numbers are generally fractional numbers. Next, we calculate the excitation energies of these two sources by calculating the kinetic energy K_i,

$$K_i=\bar{n}_i \int_i \left[\frac{p^2}{2m}\right] d\mathbf{p} \quad (i=p \text{ or } t) , \tag{4}$$

where the integration is performed for the sum of shaded and dotted areas for the projectile source or the target source. The excitation energies are obtained from K_i by correcting the Fermi energy. We denote by $E_p^{(0)}$ the excitation energy of the projectile source (particles and holes added) and by $E_t^{(0)}$ that of the target source. Finally, we calculate the total linear momenta of both sources as

$$\mathbf{P}_i^{(0)}=\bar{n}_i \int_i \mathbf{p}\cdot d\mathbf{p} \quad (i=p \text{ or } t) , \tag{5}$$

where the integration is performed for the sum of shaded and dotted areas. These two sets of parameters $\{N_p^{(0)},E_p^{(0)},\mathbf{P}_p^{(0)}\}$ and $\{N_t^{(0)},E_t^{(0)},\mathbf{P}_t^{(0)}\}$ are used as starting values of the exciton-model calculations.

B. Double-differential cross section

In the following exciton-model calculations, we assume two groups of excitons, projectile source and target source, which evolve according to the master equation independently to the equilibrium. Fast particles are emitted from an exciton state of either of the two sources. We need to first fix the change of the excitation energy E_i and momentum $\mathbf{P}_i$ $(i=p,t)$ of the two sources as the exciton number increases due to the two body collision. We impose that E_i is constant independent of the exciton number. Defining $\mathbf{P}_i(N_i)$ as the momentum vector for the source i when the exciton number is N_i, we impose that

$$\mathbf{P}_i(N_i)=\mathbf{P}_i^{(0)}\left[1-\frac{(N_i-N_i^{(0)})}{(N_i^{\mathrm{eq}}-N_i^{(0)})}\right] , \tag{6}$$

where N_i^{eq} is the equilibrium number of the excitons in the source i for given E_i, and $N_i^{(0)}$ and $\mathbf{P}_i^{(0)}$ are defined in Eqs. (3) and (5), respectively. Equation (6) means that, at equilibrium, the linear momentum is assumed to become zero due to the two body collision. The slight change of the form of Eq. (6) is found not to cause a notable change in the final result.

The evolution of the system is assumed to be governed by the same type of master equation as is used in light-ion reactions[18–20] where one imposes the never-come-back approximation for simplicity. In our case, the projectile source and the target source follow this equation independently. The double-differential cross section is written in the form

$$\frac{d^2\sigma}{d\epsilon\, d\Omega}=\sigma_{\mathrm{fus}}\sum_n \{[\tau_n W_n(\epsilon,\Omega)]_p+[\tau_n W_n(\epsilon,\Omega)]_t\} , \tag{7}$$

where σ_{fus} is the fusion cross section of two heavy ions, $\sum_n$ is the sum over the exciton number n, τ_n is the duration time of the n-exciton state (including the depletion factor), and $W_n(\epsilon,\Omega)$ is the emission rate of the particle of energy ϵ to the direction Ω from the n-exciton state. The first term within the curly braces on the right hand side of Eq. (7) is the emission from the projectile source and the second term is that from the target source. Duration time τ_n is calculated by solving the master equation of the standard type as was done in Ref. 19. To calculate the emission rate $W_n(\epsilon,\Omega)$ we use a method similar to that used by Mädler and Reif.[21] That is, we assume the capture cross section for the nucleon of energy ϵ to have the form

$$\sigma_{\mathrm{cap}}=\frac{2\pi}{\hbar}\,|M|^2\omega(\mathrm{p,h},E,\mathbf{P})d\mathbf{P}\frac{V}{v} , \tag{8}$$

where $|M|^2$ is the average value of the square of the matrix element which connects the nucleon state outside the nucleus to that inside the nucleus with the total linear momentum $\mathbf{P}$ fixed. The level density of the particle-hole (p-h) state with energy E in the momentum volume element $d\mathbf{P}$ at linear momentum $\mathbf{P}$ is written as $\omega(\mathrm{p,h},E,\mathbf{P})d\mathbf{P}$, V is the volume, and v is the velocity of the particle. The emission rate dw for the nucleon of momentum $\mathbf{p}$ is written as

$$dw=\frac{2\pi}{\hbar}(|M|^2)'\omega(\mathrm{p}-1,\mathrm{h},E-\epsilon-Q,\mathbf{P}-\mathbf{p}) \times d(\mathbf{P}-\mathbf{p})\frac{(2s+1)d\mathbf{p}\,V}{(2\pi\hbar)^3} , \tag{9}$$

where $(|M|^2)'$ is the average value of the square of the matrix element which connects the state inside the nucleus to that outside. The energy of the particle is written as ϵ, the Q value of the emission process as Q, the spin of the particle as s, and the volume of the space as V. According to the same assumption as the angle-independent exciton model, we set

$$(|M|^2)'=|M|^2 . \tag{10}$$

From Eqs. (8)–(10) we can derive the expression for the emission rate of the nucleons of energy ϵ to the direction Ω as

$$W_n(\epsilon,\Omega)=\frac{2s+1}{\pi^2\hbar^3}m\epsilon\sigma_{\mathrm{cap}}\frac{\omega(\mathrm{p}-1,\mathrm{h},E-\epsilon-Q,\mathbf{P}-\mathbf{p})}{4\pi\omega(\mathrm{p,h},E,\mathbf{P})} \times\frac{|\mathbf{P}-\mathbf{p}|^2 d(|\mathbf{P}-\mathbf{p}|)}{P^2dP} . \tag{11}$$

In deriving this equation, we assumed that the $\mathbf{p}$ dependence of $\omega(\mathrm{p,h},E,\mathbf{p})$ is only through its absolute value $p=|\mathbf{p}|$, which will be explained in the next subsection.

C. Momentum dependent level density

Now we specify the quantity $\omega(\mathrm{p,h},E,\mathbf{P})$ which appeared in Eq. (8). We start from the calculation of the quantity $\Omega(\mathrm{p,h},E,P_z)$ where we fix the z component P_z of the linear momentum $\mathbf{P}$ instead of $\mathbf{P}$ itself. Ω is given by the definition

$$\Omega(\mathrm{p,h},E,P_z)=\sum_i \delta(E-E_i)\delta(P_z-(P_z)_i) , \tag{12}$$

where δ stands for the delta function, E_i the energy of the ith level, and $(P_z)_i$ the z component of the linear momen-

tum of the ith level. Adopting the independent-particle model, the energy E_i and momentum $(P_z)_i$ are written as

$$E_i=\sum_{\epsilon(\nu)>\epsilon_F}[n(\nu)]_i\epsilon(\nu)-\sum_{\epsilon(\nu)<\epsilon_F}[n(\nu)]_i\epsilon(\nu) \tag{13}$$

and

$$(P_z)_i=\sum_{\epsilon(\nu)>\epsilon_F}[n(\nu)]_i p_z(\nu)-\sum_{\epsilon(\nu)<\epsilon_F}[n(\nu)]_i p_z(\nu)\ , \tag{14}$$

where we denote the single-particle energy of the νth level by $\epsilon(\nu)$ and its z component of the momentum by $p_z(\nu)$. The occupation number $n(\nu)$ of the νth level is understood here as the occupation number of the particle for $\epsilon(\nu)>\epsilon_F$ and as the occupation number of the hole for $\epsilon(\nu)<\epsilon_F$.

We denote the Laplace transform of Ω by $Z(\beta,\gamma)$; it is given by

$$\begin{aligned}Z(\beta,\gamma)&=\int dE\int dP_z\Omega(\mathrm{p,h},E,P_z)\exp(-\beta E-\gamma P_z)\\&=\sum_i\exp[-\beta E_i-\gamma(P_z)_i]\ .\end{aligned} \tag{15}$$

Inserting Eqs. (13) and (14) into Eq. (15), we get

$$Z(\beta,\gamma)=\sum_i\exp\left\{\sum_\nu[n(\nu)]_i[\mp\beta\epsilon(\nu)\mp\gamma p_z(\nu)]\right\}, \tag{16}$$

where $\mp$ means minus for $\epsilon(\nu)>\epsilon_F$ and plus for $\epsilon(\nu)<\epsilon_F$. For a fixed number of particles p and holes h,

$$\begin{aligned}Z(\beta,\gamma)=&\frac{1}{\mathrm{p!}}\left\{\sum_\nu\exp[-\beta\epsilon(\nu)-\gamma p_z(\nu)]\right\}^{\mathrm{p}}\\&\times\frac{1}{\mathrm{h!}}\left\{\sum_\nu\exp[\beta\epsilon(\nu)+\gamma p_z(\nu)]\right\}^{\mathrm{h}},\end{aligned} \tag{17}$$

where we neglect the effect of the Pauli principle for the occupation of the single-particle level. Introducing the quantity $g(\epsilon,p_z)$ by demanding that $g(\epsilon,p_z)d\epsilon\,dp_z$ is the number of levels in the interval $\epsilon\sim\epsilon+d\epsilon$ and $p_z\sim p_z+dp_z$, we replace the summation in Eq. (17) with the integration with respect to the energy and z component of the linear momentum,

$$Z(\beta,\gamma)=\frac{1}{\mathrm{p!}}\left[\int_{\epsilon_F}^{\infty}d\epsilon\int dp_z g(\epsilon,p_z)\exp(-\beta\epsilon-\gamma p_z)\right]^{\mathrm{p}}\frac{1}{\mathrm{h!}}\left[\int_{-\infty}^{\epsilon_F}d\epsilon\int dp_z g(\epsilon,p_z)\exp(+\beta\epsilon+\gamma p_z)\right]^{\mathrm{h}}. \tag{18}$$

The above double integral is calculated in the following manner. We define and calculate the quantity I_1 as

$$\begin{aligned}I_1&=\int dp_z g(\epsilon,p_z)\exp(-\gamma p_z)\\&=\int dp_z g(\epsilon,p_z)\left[1-\frac{\gamma}{1!}p_z+\frac{\gamma^2}{2!}p_z^2-\cdots\right]\\&=\int dp_z g(\epsilon,p_z)\left[1+\frac{\gamma^2}{2!}p_z^2+\frac{\gamma^4}{4!}p_z^4+\cdots\right].\end{aligned} \tag{19}$$

The third line follows because $g(\epsilon,p_z)$ is thought to be an even function of p_z. It is rewritten in the form

$$I_1=g(\epsilon)\left[1+\frac{\gamma^2}{2!}\langle p_z^2\rangle+\frac{\gamma^4}{4!}\langle p_z^4\rangle+\cdots\right], \tag{20}$$

where the average value of p_z^{2m} is denoted by $\langle p_z^{2m}\rangle$ and the level density $g(\epsilon)$ is defined as

$$g(\epsilon)=\int dp_z g(\epsilon,p_z)\ . \tag{21}$$

The value of $\langle p_z^{2m}\rangle$ is calculated approximately in the Appendix as

$$\langle p_z^{2m}\rangle=\frac{p_0^{2m}}{2m+1}\ , \tag{22}$$

where p_0 is the average magnitude of the linear momentum. In the numerical calculation, we use two values of p_0; i.e., p_0^+ for the particle state and p_0^- for the hole state. They are defined as

$$p_0^+=[2m(\epsilon_F+e^*)]^{1/2} \tag{23}$$

and

$$p_0^-=[2m(\epsilon_F-e^*)]^{1/2}\ , \tag{24}$$

where e^* is the average excitation energy per particle or hole. This quantity is determined once the system and its incident energy and the numbers of particles and holes are given. Substituting Eq. (22) into Eq. (20), we get

$$\begin{aligned}I_1&=g(\epsilon)\left[1+\frac{\gamma^2}{2!3}(p_0^+)^2+\frac{\gamma^4}{4!5}(p_0^+)^4+\cdots\right]\\&=\frac{g(\epsilon)}{\gamma p_0^+}\sinh(\gamma p_0^+)\ .\end{aligned} \tag{25}$$

Similarly, we can calculate another term in Eq. (18) for holes,

$$\begin{aligned}I_2&=\int dp_z g(\epsilon,p_z)\exp(+\gamma p_z)\\&=\frac{g(\epsilon)}{\gamma p_0^-}\sinh(\gamma p_0^-)\ ,\end{aligned} \tag{26}$$

where the level density $g(\epsilon)$ is taken as the same as that for particles. Substituting Eqs. (25) and (26) into Eq. (18), we are left with the integration with respect to energy. As usual, we assume that the level density $g(\epsilon)$ is constant for the region of interest and denote it with g_0. Finally, we get

$$Z(\beta,\gamma)=\frac{1}{\mathrm{p}!}\left[g_0\frac{\exp(-\beta\epsilon_F)}{\beta}\frac{\sinh(\gamma p_0^+)}{\gamma p_0^+}\right]^{\mathrm{p}} \times\frac{1}{\mathrm{h}!}\left[g_0\frac{\exp(\beta\epsilon_F)}{\beta}\frac{\sinh(\gamma p_0^-)}{\gamma p_0^-}\right]^{\mathrm{h}} . \quad (27)$$

The level density $\Omega(\mathrm{p},\mathrm{h},E,p_z)$ is obtained by the inverse Laplace transform of the quantity $Z(\beta,\gamma)$, as is seen from Eq. (15):

$$\Omega(\mathrm{p},\mathrm{h},E,p_z)=\frac{1}{(2\pi i)^2}\int_{-i\infty}^{i\infty}d\beta\int_{-i\infty}^{i\infty}d\gamma\, Z(\beta,\gamma) \times\exp(\beta E+\gamma p_z) . \quad (28)$$

Inserting Eq. (27) into Eq. (28), we get

$$\Omega(\mathrm{p},\mathrm{h},E,p_z)=\left\{\frac{(g_0)^{\mathrm{p}+\mathrm{h}}}{\mathrm{p}!\mathrm{h}!}\frac{1}{2\pi i}\int_{-i\infty}^{i\infty}d\beta\frac{\exp[-(\mathrm{p}-\mathrm{h})\epsilon_F\beta+\beta E]}{\beta^{\mathrm{p}+\mathrm{h}}}\right\} \times\left\{\frac{1}{2\pi i}\int_{-i\infty}^{i\infty}d\gamma\left[\frac{\sinh(\gamma p_0^+)}{\gamma p_0^+}\right]^{\mathrm{p}}\left[\frac{\sinh(\gamma p_0^-)}{\gamma p_0^-}\right]^{\mathrm{h}}\exp(\gamma p_z)\right\} . \quad (29)$$

This integration is calculated by the saddle-point method. The first term in Eq. (29) reduces to

$$\frac{g_0^{\mathrm{p}+\mathrm{h}}}{\sqrt{2\pi}}\frac{\exp(\mathrm{p}+\mathrm{h})}{\sqrt{\mathrm{p}+\mathrm{h}}\,\mathrm{p}!\mathrm{h}!}\left[\frac{E-(\mathrm{p}-\mathrm{h})\epsilon_F}{\mathrm{p}+\mathrm{h}}\right]^{\mathrm{p}+\mathrm{h}} . \quad (30)$$

After using the asymptotic form of the gamma function, which is valid for $\mathrm{p}+\mathrm{h}\gg 1$, Eq. (30) is rewritten in the currently used form of the Ericson's formula,[22]

$$\frac{g_0^{\mathrm{p}+\mathrm{h}}[E-(\mathrm{p}-\mathrm{h})\epsilon_F]^{\mathrm{p}+\mathrm{h}-1}}{\mathrm{p}!\mathrm{h}!(\mathrm{p}+\mathrm{h}-1)!} . \quad (31)$$

The second term in curly braces in Eq. (29) is also calculated by the saddle-point method. It involves a rather lengthy expression and we do not show it here. The saddle point is determined numerically in this case. Because of the approximation used, the level density is a product of the Ericson formula and a momentum-dependent part. It makes the calculation easier and more transparent.

Up to now, we calculated the level density for fixed p, h, E, and P_z; we wish to obtain that for fixed p, h, E, and $\mathbf{P}$. The relation between $\Omega(\mathrm{p},\mathrm{h},E,p_z)$ and $\omega(\mathrm{p},\mathrm{h},E,\mathbf{P})$ is obtained from

$$\int\Omega(\mathrm{p},\mathrm{h},E,P_z)dP_z=\int\omega(\mathrm{p},\mathrm{h},E,\mathbf{P})d\mathbf{P} . \quad (32)$$

The volume element $d\mathbf{P}$ is expressed with the nonorthogonal coordinates (P,P_z,ϕ) by

$$d\mathbf{P}=P\,dP\,P_z\,d\phi , \quad (33)$$

where ϕ is the angle of the projection of $\mathbf{P}$ to the (P_x,P_y) plane measured from the P_x axis. From the uniformity of the space, the level density $\omega(\mathrm{p},\mathrm{h},E,\mathbf{P})$ depends only on $P=|\mathbf{P}|$. Thus we get, from Eq. (32),

$$\int\Omega(\mathrm{p},\mathrm{h},E,P_z)dP_z=\int\left\{2\pi\int[\omega(\mathrm{p},\mathrm{h},E,\mathbf{P})P]dP\right\}dP_z . \quad (34)$$

From this relation, we obtain

$$\Omega(\mathrm{p},\mathrm{h},E,P_z)=2\pi\int_{P_z}^{\infty}[\omega(\mathrm{p},\mathrm{h},E,\mathbf{P})P]dP . \quad (35)$$

Finally, we come to the expression

$$\omega(\mathrm{p},\mathrm{h},E,\mathbf{P})=-\frac{1}{2\pi P}\frac{d\Omega(\mathrm{p},\mathrm{h},E,P_z)}{dP_z}\bigg|_{P_z=P} . \quad (36)$$

The derivative with respect to P_z is performed numerically. From this equation, we get the level density which depends on $|\mathbf{P}|$. Characteristics of the momentum dependence will be discussed in the next section.

III. NUMERICAL CALCULATIONS AND DISCUSSIONS

A. General remarks

Before calculating the double-differential cross section, we discuss the behavior of our momentum-dependent level density given by Eq. (36). As Eq. (29) shows, our level density is the product of the Ericson formula and the momentum-dependent term. The former is well known and we discuss here only the latter term. The inverse Laplace transform appearing in the second term in curly braces of Eq. (29) is performed with the saddle-point method. The value of γ which gives the saddle point is obtained numerically. Physically, this value is the measure of the average value of the z component of the linear momentum per excitons. After calculating this integral, the $\mathbf{P}$-dependent level density is obtained by the numerical derivative given in Eq. (36). In Fig. 2 we show one of the examples of this level density (the multiplication factor of Ericson's formula). The excitation energy dependence comes from Eqs. (23) and (24). In Fig. 2 we see a monotonic decrease of the level density as a function of the momentum. Because we use the approximation of Eqs. (23) and (24), the level density becomes negligible when the relation

$$P\geqq\mathrm{p}p_0^+ +\mathrm{h}p_0^- \quad (37)$$

holds. In Fig. 2 the initial value of the linear momentum for the reaction $^{16}\mathrm{O}+^{197}\mathrm{Au}$ is shown by the arrow on the abscissa. When the fast particle is emitted in the forward direction, the absolute value of the momentum of the residual nucleus is decreased from that of the compound nucleus and, correspondingly, the level density increases as seen in Fig. 2. (On the other hand, if the fast particle is

emitted in the backward direction, the absolute value of the linear momentum of the residual nucleus increases from that of the compound nucleus and the resulting level density decreases.) The cross section for past particle emission is proportional to the level density of the residual nucleus [see Eqs. (7) and (11)]. Therefore we have explained in our model why fast particles are preferentially emitted in the forward direction.

For the calculation of the double-differential cross section, we use the model given in the preceding section. Our model corresponds to the incomplete fusion reaction and thus the coincident measurement of the fusion residue and the fast particle is suitable for comparison. In these data, however, the fusion residue is measured at a fixed angle coincident with the energy-angle double-differential cross sections of light particles. It is impossible to calculate such triple-differential cross sections in our model. Thus we choose the data of energy-angle double-differential cross sections of light particles where the fusion residue is not measured, but the dominant reaction channel is thought to be the incomplete fusion reaction.

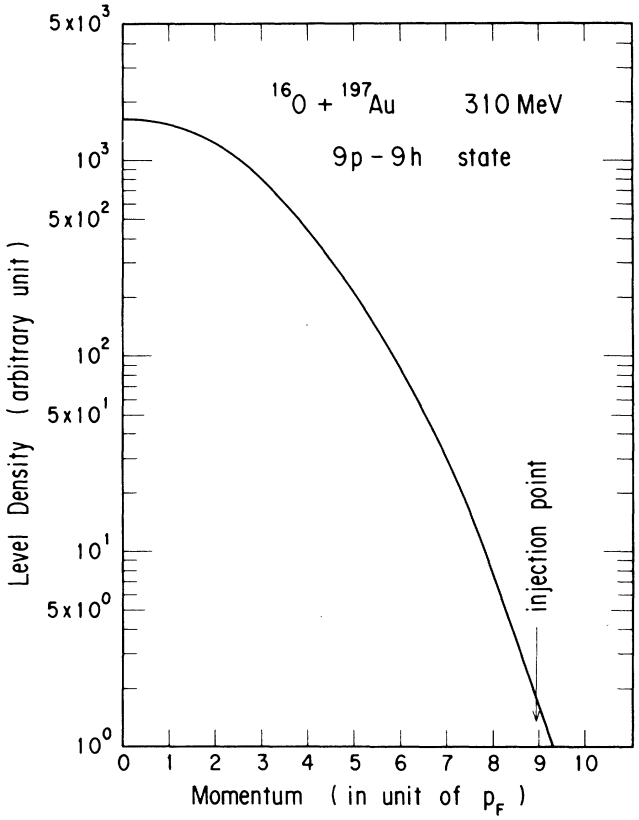

FIG. 2. Momentum-dependent part of the level density $\omega(\mathrm{p,h},E,\mathbf{P})$ as a function of the momentum $\mathbf{P}$. It is for the 9p-9h state corresponding to the excitation energy of the projectile source of the reaction 310-MeV ^{16}O on ^{197}Au. Abscissa is plotted in multiples of the Fermi momentum p_F and ordinate is plotted in arbitrary units. Initial linear momentum of the reaction is located at the arrow of injection point.

B. Values of the parameters

We give in this subsection the values of the parameters used in the calculation. Because we are interested in fast particle emission, we solve the master equation by using the never-come-back approximation in order to get the duration time τ_n in Eq. (7). From numerical calculations, this approximation appears to be adequate. We include the terms in the summation in Eq. (7) up to the first five steps of the exciton number. Addition of higher terms only affects the low energy part of the spectrum.

In order to solve the master equation, we need the spreading width $\Gamma_n^{\downarrow}$ and the escape width $\Gamma_n^{\uparrow}$ of the n-exciton state. The spreading width is assumed to have the form

$$\Gamma_n^{\downarrow}=2\pi\,|M|^2\frac{g_0^3E^2}{2(n+1)}\ , \tag{38}$$

and the value of the matrix element $|M|$ is taken from Ref. 23. The escape width is assumed to be the sum of the proton escape width and the neutron escape width. Each one is obtained from detailed balance arguments and the expression is

$$\Gamma_n^{\uparrow(i)}=\hbar\int_0^{E-B^{(i)}}d\epsilon\,\frac{2s+1}{\pi^2\hbar^3}\times u\,\epsilon\sigma_{\mathrm{cap}}^{(i)}\frac{\omega(\mathrm{p}-1,\mathrm{h},E-\epsilon-Q^{(i)})}{\omega(\mathrm{p,h},E)}\ , \tag{39}$$

where i denotes proton or neutron, $B^{(i)}$ is the binding energy, and $Q^{(i)}$ is the emission Q value. The level density $\omega(\mathrm{p,h},E)$ is assumed to be the Ericson form with the correction factor of Ref. 24. The capture cross section appearing in Eqs. (11) and (39) is taken as

$$\sigma_{\mathrm{cap}}=\pi[r_0(A_1+A_2)^{1/3}]^2\left[1-\frac{V_c}{\epsilon}\right]\ , \tag{40}$$

where

$$V_c=\frac{(Z_1+Z_2-1)e^2}{r_c(A_1+A_2-1)^{1/3}}\quad\text{for protons} \tag{41a}$$

and

$$V_c=0\quad\text{for neutrons}\ . \tag{41b}$$

Here, A_1,A_2,Z_1,Z_2 are masses and charges of the projectile and target. The values of the radius parameters are taken as

$$r_0=1.3\ \text{fm} \tag{42a}$$

and

$$r_c=1.5\ \text{fm}\ . \tag{42b}$$

In order to get the final cross section, we should also fix the fusion cross section σ_{fus} appearing in Eq. (7). It is set to the form

$$\sigma_{\mathrm{fus}}=\pi[r_0(A_1^{1/3}+A_2^{1/3})]^2\left[1-\frac{V_c'}{E}\right]\ , \tag{43}$$

TABLE I. Parameters of the initial state of the exciton model. For six reactions listed, we show the values of the particle and hole numbers $N_p^{(0)}, N_h^{(0)}$ (numbers in parentheses are those used in the exciton model calculation; see text), excitation energies of particles and holes, $E_p^{(0)}$ and $E_h^{(0)}$, in MeV, and the linear momenta of the particles and holes, $P_p^{(0)}$ and $P_h^{(0)}$, divided by the Fermi momentum.

System	Energy (MeV)	$N_p^{(0)}$ $N_h^{(0)}$	$E_p^{(0)}$ $E_h^{(0)}$	$P_p^{(0)}$ $P_h^{(0)}$
$^{16}O+^{27}Al$	215	4.48(5)	45.4	3.87
		4.48(5)	31.1	2.18
	310	5.44(6)	70.0	4.94
		5.44(6)	44.0	2.44
$^{16}O+^{90}Zr$	215	5.54(7)	73.0	5.06
		5.54(7)	45.5	2.46
	310	6.88(9)	120.6	6.76
		6.88(9)	66.4	2.69
$^{16}O+^{197}Au$	215	5.39(7)	68.7	4.89
		5.39(7)	43.4	2.43
	310	6.99(9)	125.2	6.90
		6.99(9)	68.2	2.71

where

$$V_c' = \frac{Z_1 Z_2 e^2}{r_c (A_1^{1/3} + A_2^{1/3})} . \tag{44}$$

The same values of the radius parameters as in Eq. (42) are used. The value of the Fermi energy ϵ_F used to calculate Eqs. (3)—(5) is set as

$$\epsilon_F = 33.5 \text{ MeV} . \tag{45}$$

Because one aim of the present investigation is to clarify the phenomenological moving-source model, we choose the experimental data of Awes *et al.*,[2] where the moving-source analysis is done thoroughly. The experiment involves the ^{16}O-induced reaction on ^{27}Al, ^{90}Zr, and ^{197}Au targets with incident energies of 215 and 310 MeV. We first show in Table I the initial state of the exciton-model calculation obtained by the method of Sec. II A. The calculated particle and hole numbers are fractional numbers and the numbers in parentheses are the starting values of the exciton model calculation. We see that the latter numbers are former numbers plus 0.5—2 exciton pairs. There is a tendency that, as the excitation energy increases and the target mass increases, the number added also increases. This number (of pairs) is the fitting parameter in our model. By comparison, in the case of light-ion reactions we usually start from a 2p-1h state, i.e., the addition of 1p-1h to the incoming nucleon.

C. Double-differential cross sections

In Figs. 3—5 we show the double-differential cross section of the six reactions given in Table I. In the calculation we first change the laboratory angle and energy to

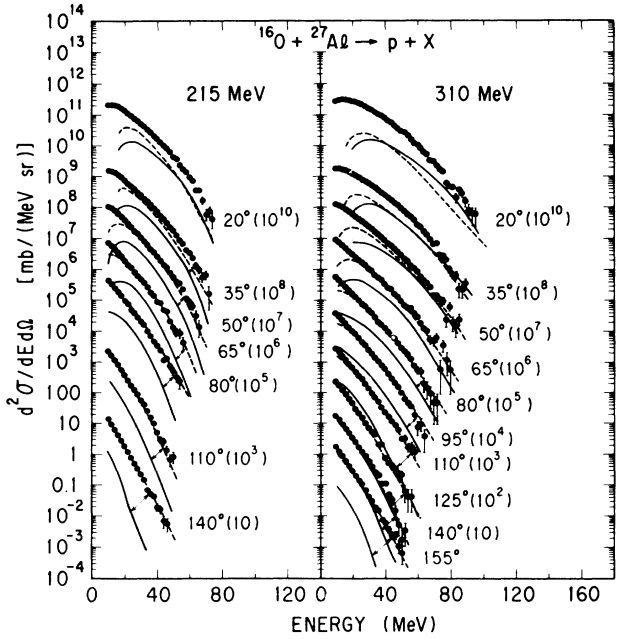

FIG. 3. Energy-angle double-differential cross section of protons in the reaction $^{27}Al(^{16}O,p)$. Left panel is for the incident energy of 215 MeV and right is for 310 MeV. Abscissa is the laboratory energy and circles are the experimental data taken from Ref. 2; solid lines are our calculations. Dashed lines are the evaporation calculations with the level density parameter of $A/20$.

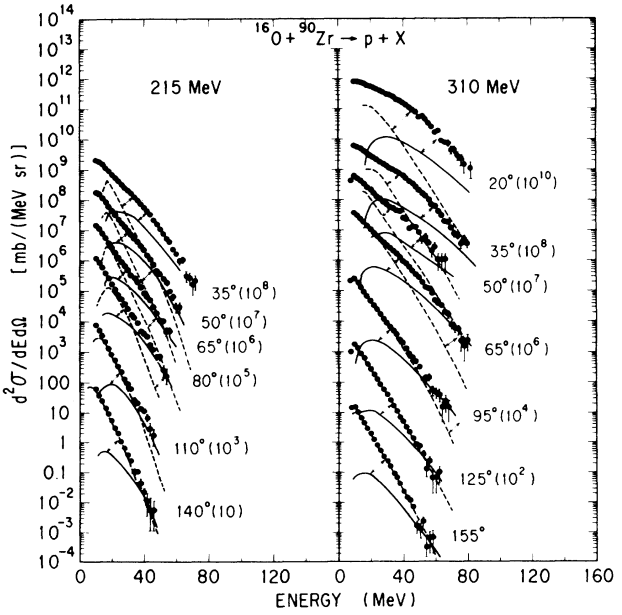

FIG. 4. Same as Fig. 3, but for the reaction $^{90}Zr(^{16}O,p)$. The evaporation calculations are performed with the level density parameter of $A/13$.

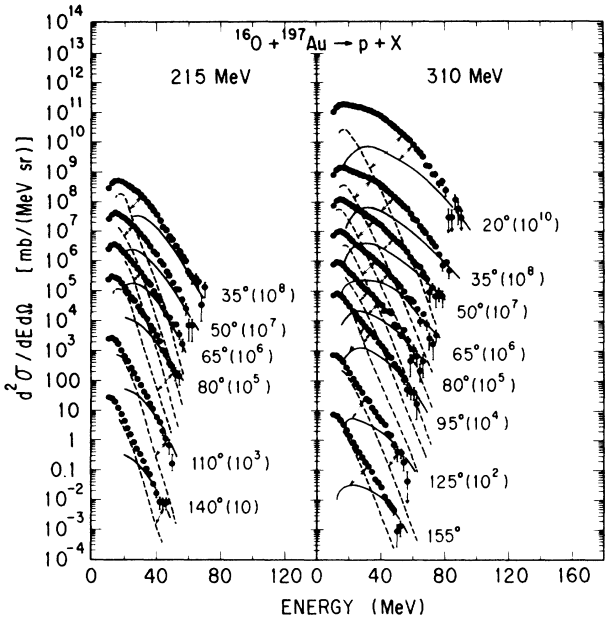

FIG. 5. Same as Fig. 2, but for the reaction $^{197}Au(^{16}O,p)$. The evaporation calculations are performed with the level density parameter of $A/13$.

those of the center of mass frame. The formulas of Sec. II are then used to calculate the double-differential cross section. We calculate the emission from the projectile source and target source independently. Numerical calculation shows that the contribution from the target source is negligible, even in the case of the Al target, where target emission is most prominent. Thus we show in Figs. 3—5 the contributions from the projectile sources only. We also include the evaporation calculation from the compound state by the dashed lines. As stated in the preceding subsection, we include only the first five steps in the excitons in our calculation and thus the evaporation part of the spectra should be added to our calculation in order to facilitate comparison with the data. To show the correspondence between the calculation and data, we draw thin lines with arrows. The level-density parameters which enter into the evaporation formula are chosen to give a good fit to the slope of the energy spectra at the extreme back angles. The value thus chosen is $A/20$ for Al; it is $A/13$ for Zr and Au targets. The normalization of the evaporation calculation is chosen to fit the backward-angle data at an emission energy of 10—20 MeV. There are systematic deviations between calculations and data at the very-low-energy region near the maxima of the cross sections. The use of the sharp cutoff of the barrier penetration factor is partly responsible for these deviations, but detailed investigation of this effect is beyond the scope of the current paper.

In the case of ^{27}Al (see Fig. 3), the evaporation calculation gives a good fit to the data for angles larger than 35° for the 215 MeV case and larger than 50° for the 310 MeV case. For these angles, our calculation gives only a fraction of the experimental data. In the cases of the 20° data for both 215 and 310 MeV and the 35° data for 310 MeV, the solid line gives imporant contributions to the high-energy part of the spectra, and adding it to the evaporation part (dashed line) greatly improves the fits. There is a tendency, however, that the calculation (absolute value) underestimates the data at low energies. This tendency is most prominent for the 20° data at 310 MeV, where the same discrepancy was seen in the moving-source parametrization given in Ref. 2, and we do not investigate it further.

For the ^{90}Zr target case shown in Fig. 4, the situation differs greatly from the ^{27}Al target case. For both 215 and 310 MeV incident energies the evaporation calculation fails to fit the data at all angles smaller than 110°. Addition of the solid line to the dashed line greatly improves the fits at high emission energy. Except for the low-emission-energy part, which has the same nature as pointed out in the preceding paragraph, the spectra are reproduced well with the calculation. Preequilibrium contribution to the cross section at high emission energy is one to two orders larger compared to the evaporation calculations. This deviation is impossible to explain by the adjustment of the level-density parameter in the evaporation calculation.[1,2] Our calculation explains the origin of the deviation naturally and the systematics of the data can be reproduced well with it.

The large contribution of the preequilibrium emission is more pronounced in the ^{197}Au target case shown in Fig. 5. The evaporation calculation with the level density parameter of $A/13$ fails to reproduce the data even at the most backward angle of 155°. Addition of the solid line to the dashed line greatly improves the fit at high emission energy. In the ^{197}Au case the enhancement of the cross section at high emission energy is more than three orders of magnitude for the forward angles and about one order for the backward angles.

From Figs. 3—5 we see that the contribution of the preequilibrium emission becomes larger as the target becomes heavier. The main change is the increase of the center-of-mass excitation energy and thus we can conclude that as the excitation energy increases the preequilibrium emission becomes more important in the energy range we examined. From Table I we see that the effective excitation energies in the Al (310 MeV), Zr (215 MeV), and Au (215 MeV) cases are similar, but the deviation from the evaporation is much larger for the latter two, as seen from Figs. 3—5. Thus, apart from the excitation energy effect, there is also the effect coming from the size of the target or, more precisely, the ratio of the target mass to the projectile mass. This effect is fully taken into account in our model because the change of this ratio causes the change in the shift of the Fermi spheres of the projectile and target, as seen in Fig. 1. At any rate, our model calculation can explain systematically the contribution of the preequilibrium emission corresponding to the change of the detection angle, change of the effective excitation energy, and target-projectile mass ratio. Because our model is simple and employed drastic approximations, we did not aim for the precise fitting of the data. We could get, however, the result which is qualitatively similar to the phenomenological moving-source parametrization. Our model is, therefore, one approach to understanding the physics of the moving source model.

IV. SUMMARY

We have formulated a model describing the preequilibrium emission of fast particles in low energy heavy-ion reactions. The model is specially developed to calculate the fast particles associated with fusion, namely the incomplete fusion reaction. For such reactions the moving-source parametrization is known to give a good fit to the data. One aim of the present investigation is to clarify the mechanism of that model on more fundamental grounds. The idea of the Fermi-jet model and the related phenomenological analysis using the Fermi-sphere considerations led us to set up the initial conditions of the calculation. After specifying this, we used the exciton model to take into account the secondary scattering of the excitons, which is hard to do in the framework of the Fermi-jet model. To calculate the angular distribution we extended the exciton model so as to use the linear momentum of the exciton system as a new variable. This linear momentum is defined separately for the projectile source and target source. The emission rate of the particle of energy ϵ in a definite direction is calculated using the level density of the excitons, which is generalized to depend not only on the particle and hole numbers and excitation energy, but also on the total linear momentum of the exciton system. This level density is similar to the commonly used angular-momentum-dependent level density.

On the basis of this model, we have performed the calculation of energy-angle double-differential cross sections for the emission of protons. Six reactions with an energy per particle of 10—20 MeV are examined. The reactions with lower incident energy and lighter target mass are found to be described almost completely by the evaporation model. Numerical calculations show that the preequilibrium particles are emitted preferentially in the forward direction and their contributions increase as the excitation energy increases and the mass of the system increases. These are just the characteristics of the experimental data, and addition of our calculation to the evaporation spectra reproduces the data systematically well. The change of the cross section with the detection angle is very similar to the phenomenological moving-source model.[1,2] Our model includes a fitting parameter which changes the initial number of the excitons, but this adjustment is only 0.5—2 pairs of particle-hole and is rather systematic. Thus we can say that, in spite of the simplicity of the model, it predicts the systematic features of fast-particle emission very well. Our method of including the linear momentum of the excitons into the level density formula is one way of explaining the phenomenological moving source model. The effect of the secondary scattering of the Fermi-jet particles is calculated by the exciton model in our calculations. Instead of calculating collision terms dynamically, as is done in the BUU or VUU model,[13,14] we take them into account phenomenologically by simple statistical assumptions.

ACKNOWLEDGMENTS

The author would like to express his thanks to Dr. K. Harada for continuous encouragement and fruitful discussions throughout this work. Helpful and clarifying discussions with Professor S. Yoshida, Dr. N. Shikazono, Dr. H. Ikezoe, Dr. T. C. Awes, and Professor W. J. Swiatecki are gratefully acknowledged. The author is indebted to Dr. S. Raman for carefully reading the original manuscript and for useful comments. He wishes to also express his appreciation to the Oak Ridge National Laboratory for its generous hospitality during a visit in which a part of this work was performed.

APPENDIX

We give here a brief deviation of Eq. (22). We use the classical approximation to obtain the expectation value of the projection of the single-particle linear momentum. The classical phase space density $g(\mathbf{p},\mathbf{r})$ is assumed to have the form

$$g(\mathbf{p},\mathbf{r})=2\left[\frac{1}{2\pi\hbar}\right]^3 . \tag{A1}$$

Because we are interested in the application to the heavy-ion reactions, the magnitude of the single-particle momenta is concentrated around the average value, as is seen in the shaded and dotted regions of Fig. 1. We denote the average magnitude of the momentum by p_0 and calculate the average value of $(p_z)^{2m}$ as

$$\langle p_z^{2m}\rangle=\frac{\int g(\mathbf{p},\mathbf{r})\delta(p^2/2M-p_0^2/2M)p_z^{2m}d\mathbf{p}\,d\mathbf{r}}{\int g(\mathbf{p},\mathbf{r})\delta(p^2/2M-p_0^2/2M)d\mathbf{p}\,d\mathbf{r}} . \tag{A2}$$

This integration is easily calculated to give the final result,

$$\langle p_z^{2m}\rangle=\frac{p_0^{2m}}{2m+1} , \tag{A3}$$

which is the result used in Eq. (22).

[1]T. C. Awes, G. Poggi, C. K. Gelbke, B. B. Back, B. G. Glagola, H. Breuer, and V. E. Viola, Jr., Phys. Rev. C **24**, 89 (1981).
[2]T. C. Awes, S. Saini, G. Poggi, C. K. Gelbke, D. Cha, R. Legrain, and G. D. Westfall, Phys. Rev. C **25**, 2361 (1982).
[3]J. P. Bondorf *et al.*, Nucl. Phys. **A333**, 285 (1980).
[4]K. T. R. Davies, B. Remaud, M. Strayer, K. R. Sandya Devi, and Y. Raffray, Ann. Phys. (N.Y.) **156**, 68 (1984).
[5]K. Moling, W. J. Swiatecki, and Z. Zielinska-Pfabe, Nucl. Phys. **A440**, 89 (1985).
[6]M. Blann, Phys. Rev. C **23**, 205 (1981).
[7]T. Otsuka and K. Harada, Phys. Lett. **121B**, 106 (1983).
[8]H. Machner, Phys. Rev. C **28**, 2173 (1983).
[9]S. Yoshida and H. Morinaga, Z. Phys. A **317**, 173 (1984).
[10]K. Niita, Z. Phys. A **316**, 309 (1984).
[11]A. S. Umar, M. R. Strayer, D. J. Ernst, and K. R. Sandhya Devi, Phys. Rev. C **30**, 1934 (1984).
[12]H. S. Köller, Nucl. Phys. **A438**, 564 (1984).
[13]J. Aichelin and G. Bertsch, Phys. Rev. C **31**, 1730 (1985).

[14]H. Kruse, B. V. Jacak, J. J. Moritoris, G. D. Westfall, and H. Stöcker, Phys. Rev. C **31**, 1770 (1985).
[15]A. Iwamoto, in *Proceedings of the 4th International Conference on Nuclear Reaction Mechanisms,* Varenna, 1985, edited by E. Gadioli (Ricerta Scientifica de Educazione Permanente, Milan, 1985), p. 51.
[16]H. Morgenstern, W. Bohne, W. Galster, K. Grabisch, and A. Kyanowki, Phys. Rev. Lett. **52**, 1104 (1984).
[17]G. S. Stephans *et al.*, Phys. Lett. **161B**, 60 (1985).
[18]J. J. Griffin, Phys. Rev. Lett. **17**, 478 (1966).
[19]L. Milazzo Colli and G. M. Marcazzan, Riv. Nuovo Cimento **3**, 535 (1973).
[20]M. Blann, Annu. Rev. Nucl. Sci. **25**, 123 (1975).
[21]P. Mädler and R. Reif, Nucl. Phys. **A337**, 445 (1980).
[22]T. Ericson, Adv. Phys. **9**, 425 (1960).
[23]C. Kalbach, Z. Phys. A **287**, 319 (1978).
[24]F. C. Williams, Jr., Nucl. Phys. **A166**, 231 (1971).